Biochemistry and Biophysics Reports 11 (2017) 99–104

Contents lists available at ScienceDirect

Biochemistry and Biophysics Reports

journal homepage: www.elsevier.com/locate/bbrep

Unveiling the folding mechanism of the Bromodomains

Maria Petrosino[a,1], Daniela Bonetti[a,1], Alessandra Pasquo[b], Laura Lori[a], Roberta Chiaraluce[a], Valerio Consalvi[a], Carlo Travaglini-Allocatelli[a,*]

[a] Dipartimento di Scienze Biochimiche "A. Rossi Fanelli", Università di Roma "Sapienza", P.le A. Moro 5, 00185 Rome, Italy
[b] SSPT-BIOAG-BIOTEC ENEA Casaccia ENEA, Rome, Italy

ARTICLE INFO

Keywords:
Bromodomain
Protein folding
Folding intermediate

ABSTRACT

Bromodomains (BRDs) are small protein domains often present in large multidomain proteins involved in transcriptional regulation in eukaryotic cells. They currently represent valuable targets for the development of inhibitors of aberrant transcriptional processes in a variety of human diseases. Here we report urea-induced equilibrium unfolding experiments monitored by circular dichroism (CD) and fluorescence on two structurally similar BRDs: BRD2(2) and BRD4(1), showing that BRD4(1) is more stable than BRD2(2). Moreover, we report a description of their kinetic folding mechanism, as obtained by careful analysis of stopped-flow and temperature-jump data. The presence of a high energy intermediate for both proteins, suggested by the non-linear dependence of the folding rate on denaturant concentration in the millisec time regime, has been experimentally observed by temperature-jump experiments. Quantitative global analysis of all the rate constants obtained over a wide range of urea concentrations, allowed us to propose a common, three-state, folding mechanism for these two BRDs. Interestingly, the intermediate of BRD4(1) appears to be more stable and structurally native-like than that populated by BRD2(2). Our results underscore the role played by structural topology and sequence in determining and tuning the folding mechanism.

1. Introduction

Proteins involved in the regulation of histone post-translational modifications, such as those involved in acetylation, phosphorylation or methylation, play a pivotal role in the control of gene expression [1], therefore acting as "proof-editors" of the genetic code. Proteins acting on the histone acetylation processes can be grouped in at least three different subsets, on the basis of their specific function: "writer" proteins (as Histone AcetylTransferases, HATs) responsible for the addition of acetyl groups to specific lysine residues, "eraser" proteins removing specific acetyl groups (as Histone DeAcetylases, HDACs), and "reader" proteins, endowed with the ability to recognize and bind to specific histone acetylated lysines (AcK), such as the Bromodomains (BRDs) [2,3].

BRDs are conserved structural motifs of about 100 amino acids that are often present in large multidomain proteins involved in a variety of cellular processes, such as chromatin remodeling, post-translational modifications or transcriptional control [4]. Members of the BET (Bromo-Extra-Terminal domain) family (comprising human BRD2, BRD3, BRD4 and BRDT) display common modular architecture with two highly conserved amino-terminal BRDs, and a less conserved C-terminal recruitment domain. Mutations or chromosomal rearrangements affecting BRDs have been linked to various human diseases including cancer, and therefore BRDs are currently considered a promising target for the development of small-molecule inhibitors aiming at interfering with aberrant transcriptional processes in such diseases [5–7].

The structure of a variety of BRDs has been solved and shows a conserved left-handed helical bundle composed by four α-helices termed αZ, αA, αB and αC (from the N-terminal to the C-terminal helix) connected by loop regions of variable length (ZA and BC loops) (Fig. 1). From a structural point of view the BRDs therefore belong to the all-α fold class. Structural analyses of acetylated peptide-BRD complexes have shown that the AcK binding site is a hydrophobic cavity present on top of the helical bundle whose surface is shaped mainly by the ZA and BC loops. Not surprisingly, given the pivotal role played by BRDs in a variety of patho-physiological processes, a growing number of studies are currently focusing on their ligand binding affinity and specificity. However, little is known about the dynamic properties of these domains and, to our knowledge, no information is available about the mechanisms of folding of BRDs. This lack of information is somewhat surprising as it is known that for many proteins a relationship exists between

* Corresponding author.
E-mail address: carlo.travaglini@uniroma1.it (C. Travaglini-Allocatelli).
[1] M.P and D.B. contributed equally for this work.

http://dx.doi.org/10.1016/j.bbrep.2017.06.009
Received 29 March 2017; Received in revised form 23 June 2017; Accepted 28 June 2017
Available online 08 July 2017

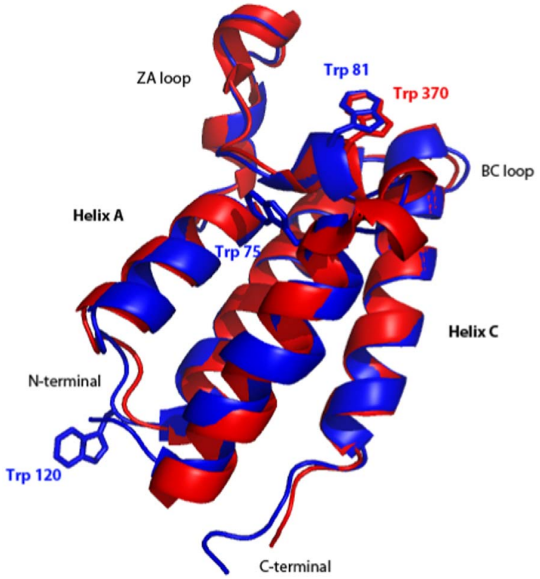

Fig. 1. Structural alignment of BRD2(2) (pdb id: 3oni), shown in red, and BRD4(1) (pdb id: 3uvx), shown in blue. The Trp residues are shown in sticks representations. BRD2(2) contains only one Trp (Trp370, structurally homologous to Trp81 of BRD4(1)); BRD4(1) presents two additional Trp residues (Trp75 and Trp120). The alignment was generated using PyMol (The PyMOL Molecular Graphics System, Version 1.8 Schrödinger, LLC).

folding and ligand binding mechanisms, e.g. in the classical induced-fit model, in the case of other small protein domains involved in mediating protein-protein interactions [8] or in the case of intrinsically disordered proteins [9,10]. Interestingly, in the case of BRD domains, a ligand-induced conformational change has been proposed and discussed [11,12]. In light of these considerations we believe that obtaining information about the folding mechanism of the BRD domains may pave the way to a better understanding of their binding mechanism.

In this report we investigate the thermodynamic properties and the folding mechanism of two BET bromodomains: the second BRD of BRD2 (hereafter, BRD2(2)) and the first BRD of BRD4 (hereafter, BRD4(1)) by equilibrium spectroscopy and pre steady-state kinetic experiments. We decided to focus on these two BET BRDs because i) they are representative of the first and second domains generally found in the BET BRD family and ii) they represent ideal experimental system to investigate conservation (if any) of the folding mechanism among members of a fold family. Indeed these two BET BRDs display a 56% sequence similarity and, as can be seen from Fig. 1, they are structurally very similar (Cα root-mean square deviation (RMSD) is 1.2 ± 0.7 Å). It should be recalled that the folding mechanism of other all-α proteins has been studied in detail [13–16], leading to the hypothesis that formation of a folding intermediate is tuned by the specific α-helical propensities.

Quantitative analyses of stopped-flow (SF) mixing experiments and ultra-rapid temperature-jump (T-jump) data, allowed us to show that the folding mechanism of both BRDs are consistent with the presence of a folding intermediate, transiently populated in the sub-milliseconds time-regime. However, our results suggest that the two intermediate species show dissimilar thermodynamic and structural properties, highlighting different dynamic properties of these two BRDs.

2. Materials and methods

2.1. Protein expression and purification

BRD2(2) and BRD4(1) were expressed in *E.coli* and purified as previously described [17] and briefly reported in the legend to Fig. S1. [17]. Structural integrity of the purified proteins was checked by CD spectra in the far- and near-UV region (Figs. S2 and S3, respectively).

2.2. Urea-induced equilibrium unfolding

All experiments were carried out at 20 °C in 20 mM Tris/HCl, pH 7.5, 0.2 M NaCl, 200 μM DTT. Intrinsic fluorescence emission measurements were carried out with a LS50B spectrofluorimeter (Perkin-Elmer) using a 1.0 cm path length quartz cuvette. Fluorescence emission spectra were recorded from 300 to 450 nm (1 nm sampling interval), with the excitation wavelength set at 295 nm. Circular dichroism (CD) measurements were performed with a JASCO J-720 spectropolarimeter using a 0.2-cm cuvette. For urea-induced equilibrium unfolding, proteins (final concentration ranging over 50.0 − 100 μg/mL) were incubated at 20 °C at increasing concentrations of urea (0 − 9.5 M). When equilibrium was reached, intrinsic fluorescence emission and far-UV CD spectra were recorded in parallel. To test the reversibility of the unfolding, BRD2(2) and BRD4(1) were denatured in 7.9 M urea at protein concentration ranging over 0.5–1.0 mg/mL. After 10 min, refolding was started by 15-fold dilution of the unfolding mixture into solutions of the same buffer used for unfolding containing decreasing urea concentrations. The final protein concentration ranged over 50.0 − 100 μg/mL. After 24 h, intrinsic fluorescence emission and far-UV CD spectra were recorded at 20 °C. All equilibrium unfolding experiments were performed in triplicate. The changes in intrinsic fluorescence emission spectra at increasing urea concentrations were quantified as the changes of the relative fluorescence intensity at 345 and at 350 nm for BRD2(2) and BRD4(1), respectively. The excitation wavelength used was 295 nm.

Urea-induced equilibrium unfolding transitions monitored by far-UV CD ellipticity and intrinsic fluorescence emission changes were analysed by fitting baseline and transition region data to a two-state linear extrapolation model [18] according to

$$\Delta G_{\mathrm{unf}} = \Delta G^{H_2O} + m[\mathrm{Urea}] - RT \ln (K_{\mathrm{unf}}) \quad (1)$$

where ΔG_{unf} is the free energy change for unfolding for a given denaturant concentration, $\Delta G_2^{\mathrm{H}\circ}$ the free energy change for unfolding in the absence of denaturant and m a slope term which quantifies the change in ΔG_{unf} per unit concentration of denaturant, R the gas constant, T the temperature and K_{unf} the equilibrium constant for unfolding. The model expresses the signal as a function of denaturant concentration:

$$y_i = \frac{y_N + s_N[X]_i + (y_U + s_U[X]_i) * \exp[(-\Delta G^{H_2O} - m[X]_i)/RT]}{1 + \exp\left[\frac{-\Delta G^{H_2O} - m[X]_i}{RT}\right]} \quad (2)$$

where y_i is the observed signal, y_U and y_N are the baseline intercepts for unfolded and native protein, s_U and s_N are the baseline slopes for the unfolded and native protein, $[X]_i$ the denaturant concentration after the i^{th} addition, $\Delta G^{H_2}O$ the extrapolated free energy of unfolding in the absence of denaturant, m the slope in a $\Delta G_{\mathrm{unfolding}}$ versus [X] plot.

The denaturant concentration at the midpoint of the transition, $[\mathrm{Urea}]_{0.5}$, according to Eq. (2), is calculated as:

$$[\mathrm{Urea}]_{0.5} = \Delta G^{H_2O}/m \quad (3)$$

2.3. Kinetic experiments

Stopped-flow kinetic folding experiments were carried out on a SX-17 stopped-flow instrument (Applied Photophysics, Leatherhead, UK) in Tris/HCl 50 mM buffer pH 7.5, 0.2 M NaCl, 2 mM DTT, at 20 °C; the excitation wavelength was 280 nm and the fluorescence emission was measured using a 320 nm cut-off glass filter. In all experiments, refolding and unfolding were initiated by a 11-fold dilution of the denatured or the native protein with the appropriate buffer. Usually 4–6 individual traces were accumulated and averaged. Final protein concentration was typically 5 μM.

Analysis was performed by non-linear least squares fitting of exponential phases using the fitting procedures provided in the Applied Photophysics software.

The relaxation kinetics was measured by using a Hi-Tech PTJ-64 capacitor-discharge T-jump apparatus (Hi-Tech, Salisbury, UK). Degassed and filtered samples were slowly pumped through the 0.5 × 2 mm quartz flow cell before data acquisition. Temperature was rapidly changed with a jump-size of 9 °C (from 11 °C to 20 °C). Usually 10–20 individual traces were accumulated and averaged. The excitation wavelength was 296 nm and the fluorescence emission was measured using a 320 nm cut-off glass filter. Protein concentration was typically 20 μM. The buffer used was Tris/HCl 50 mM buffer pH 7.5, 0.2 M NaCl, 200 μM DTT.

Experimental kinetic data were modeled on the basis of a three-state folding scheme, either with an on- or off-pathway intermediate, assuming that the logarithm of the microscopic rate constants linearly depends on the denaturant concentration: $\ln k_{ij} = \ln k_{ij}^{\circ} + m_{ij}(RT)^{-1}[\text{urea}]$, where k_{ij}° and m_{ij} represent the elementary rate constant in the absence of urea and the urea dependence of the rate constant (kinetic m value), 205 [19, 20].

For the two step reaction, global analysis of the two apparent rate constants λ_1 and λ_2 was performed by non-linear least-squares fitting of the kinetic data as previously described [19] using Graphpad Prism 5.04.

Kinetic ΔG values were calculated as follows: $\Delta G_{DN} = -RT \ln (k_{DI} \times k_{IN}) / (k_{ID} \times k_{NI})$; $\Delta G_{DI} = -RT \ln k_{DI} / k_{ID}$. Tanford β-values ($\beta_T$) were calculated as follows: $\beta_T(D) = 0$; $\beta_T(TS1) = -m_{DI}/m_{DN}$; $\beta_T(I) = (m_{ID} - m_{DI})/m_{DN}$; $\beta_T(TS2) = 1 - m_{NI}/m_{DN}$; $\beta_T(N) = 1$; m_{DN} is the kinetically derived 'equilibrium' m value, $m_{DN} = m_{ID} - m_{DI} + m_{NI} - m_{IN}$.

3. Results and discussion

3.1. Urea-induced equilibrium unfolding

The thermodynamic stability of BRD2(2) and BRD4(1) was determined at pH 7.5 and 20 °C by urea-induced equilibrium unfolding experiments, monitoring both the change of ellipticity at 222 nm by CD spectroscopy (Fig. 2A) and the change of intrinsic fluorescence emission (Fig. 2B). In all cases, the observed unfolding transitions were checked for reversibility. The same samples used to monitor the far-UV CD changes during the unfolding transition were used to monitor fluorescence emission changes, to allow a direct comparison of the data.

For both proteins, the denaturation curves obtained by monitoring the CD signal at 222 nm are satisfactorily fitted to a two-state model. The calculated unfolding free energy in water (ΔG^{H_2O}) for BRD2(2) is 8.83 ± 0.59 kcal mol^{-1} and the m value is 1.93 ± 0.13 kcal mol^{-1} M^{-1}, while for BRD4(1) the same thermodynamic parameters are ΔG^{H_2O} = 11.52 ± 0.65 kcal mol^{-1} and m = 1.67 ± 0.09 kcal mol^{-1} M^{-1}, highlighting a larger stability for BRD4(1) compared to BRD2(2) ($\Delta\Delta G$ = 2.69 kcal mol^{-1}) (Table 1).

In the case of BRD2(2), fitting the unfolding transition obtained by monitoring the changes of the fluorescence emission intensity to a two-state model allowed us to obtain thermodynamic parameters comparable to those obtained by CD (ΔG^{H_2O} = 9.09 ± 0.68 kcal mol^{-1}, m = 1.81 ± 0.13 kcal mol^{-1} M^{-1}). However, in the case of BRD4(1), the unfolding transition obtained by monitoring the fluorescence changes could not be fitted to a two-state model because of a multiphasic profile (Fig. 2B). This result can be explained by the observation that BRD4(1), contrary to BRD2(2), contains more than one Trp residues, each monitoring the conformational properties of different regions of the protein (Fig. 1). Indeed, the different molecular environment of the fluorophores in the two BRDs is also mirrored by the different fluorescence emission spectra of their relative native states shown in Fig. S4.

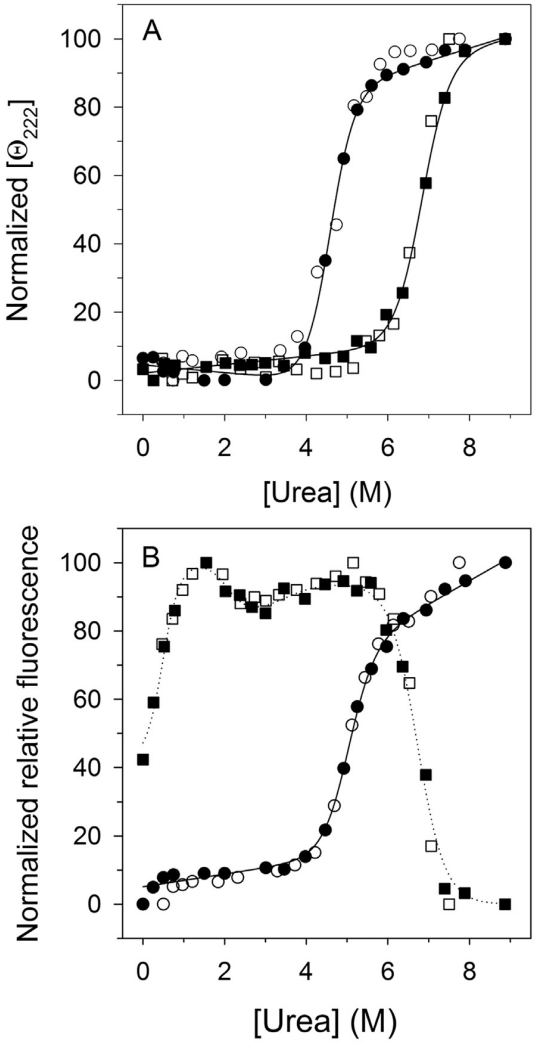

Fig. 2. Urea-induced equilibrium unfolding of BRD2(2) and BRD4(1). (A) Normalized molar ellipticity at 222 nm ($[\Theta]_{222}$) of BRD2(2) (circles) and BRD4(1) (squares) reported after removal of the high-frequency noise and the low-frequency random error by SVD. Continuous lines are the nonlinear regression to Eq. 2 of the data at different denaturant concentrations, as described in Section 2. (B) Normalized relative intrinsic fluorescence changes of BRD2(2) (circles) and BRD4(1) (squares). Continuous lines are the nonlinear regression of the data at different denaturant concentrations fitted according to Eq. 2 for BRD2(2), as described in Section 2. The dotted line interpolating the relative fluorescence intensity for BRD4(1) (squares) is drawn as a guide to the eye. The reversibility points (empty symbols) were not included in the nonlinear regression analysis.

Table 1
Thermodynamic parameters for urea-induced unfolding equilibrium of BRD2 (2) and BRD4 (1) measured by far-UV CD and fluorescence spectroscopy.

	BRD2(2)		BRD4(1)
	CD ($[\Theta]_{222}$)	Fluorescence	CD ($[\Theta]_{222}$)
$\Delta G_2^{H_2O}$ (kcal/mol)	8.83 ± 0.59	9.09 ± 0.68	11.52 ± 0.65
m (kcal/mol/M)	1.93 ± 0.13	1.81 ± 0.13	1.67 ± 0.09
$[\text{Urea}]_{0.5}$ (M)	4.57	5.02	6.90

Urea-induced unfolding equilibrium data were obtained as described in Materials and methods. Data are reported as the mean ± SE of the fit. For BRD4(1) fluorescence changes could not be fitted to a two-state model because of a multiphasic profile (Fig. 2 B).

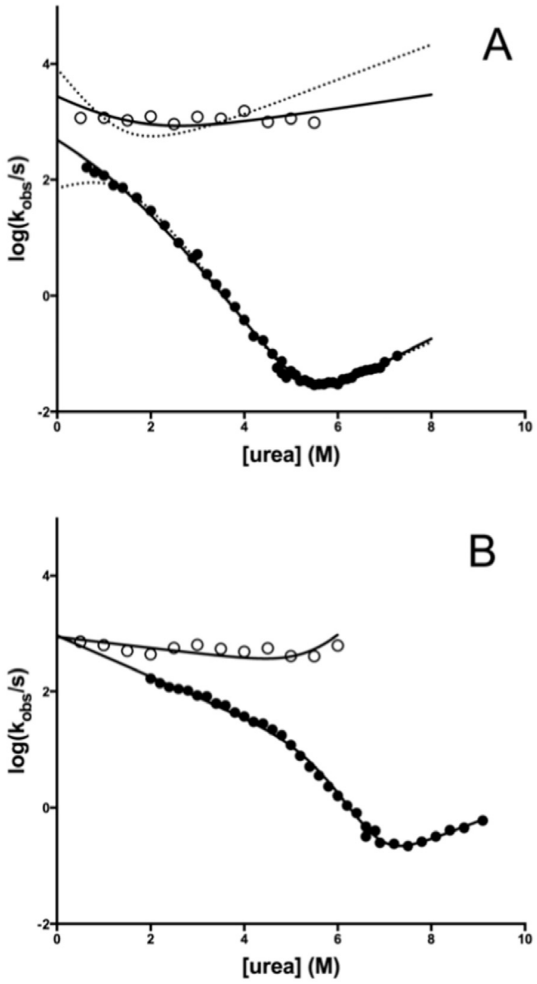

Fig. 3. Semilogarithmic plot (chevron plot) of the observed folding and unfolding rate constants as a function of urea concentration by SF (closed symbols) and T-jump (open symbols) experiments for BRD2(2) (panel A) and BRD4(1) (panel B). In panel A, the lines are the best fit to a three-state model involving on- (continuous line) or off-pathway (dashed line) intermediates [19]. BRD2(2) (Panel A): the calculated parameters for the on-pathway model are are: k_{DI} = 2357 ± 831; m_{DI} = 0.60 ± 0.33; k_{ID} = 329 ± 163; m_{ID} = 0.16 ± 0.06; k_{IN} = 570 ± 211; m_{IN} = 0.58 ± 0.34; k_{NI} = 0.00010 ± 0.00008; m_{NI} = 0.53 ± 0.07. BRD4(1) (Panel B): the calculated parameters for the on-pathway model (continuous line) are are: k_{DI} = 924 ± 130; m_{DI} = 0.47 ± 0.02; k_{ID} = 0.007 ± 0.010; m_{ID} = 1.12 ± 0.15; k_{IN} = 875 ± 115; m_{IN} = 0.12 ± 0.02; k_{NI} = 0.001 ± 0.001; m_{NI} = 0.40 ± 0.08. Rate constants are in s^{-1} and the associated m values are in kcal mol^{-1} M^{-1}. In the case of BRD4(1) the fit to an off-pathway model does not converge.

3.2. Kinetic folding-unfolding experiments

To gain information on the folding mechanism of these two BRDs, we carried out kinetic folding experiments at pH 7.5, 20 °C by fluorescence-monitored SF and T-jump experiments. The unfolding time courses obtained by rapid-mixing SF experiments for BRD2(2) and BRD4(1) were satisfactorily fitted to a single exponential decay at any final denaturant concentration (see Fig. S5A and S5B for representative unfolding time courses), while the refolding reaction was characterized by two processes having relaxation constants in different time regime (at [urea] around 1 M, k_1 ~100 s^{-1} and k_2 ~1 s^{-1}) (see Fig. S5C and S5D for representative refolding time courses). Since the slower refolding phase is characterized by a smaller amplitude (less than 10% of the faster phase) and is largely independent on denaturant concentration, it probably originates from *cis-trans* proline isomerization, as often observed in the folding of other proteins [21]

Fig. 3 shows the semi-logarithmic plot of the observed folding/unfolding rate constants (excluding the slow proline isomerization folding phase) *versus* denaturant concentration (chevron plot) obtained for BRD2(2) (Fig. 3A) and BRD4(1) (Fig. 3B) from SF (closed symbols) and T-jump (open symbols) experiments (see below). It should be noticed that, whereas the logarithm of the observed unfolding rate constant increases linearly with increasing denaturant concentration, both BRDs show a deviation from linearity of the observed refolding rate constants obtained by SF at low urea concentrations (roll-over effect). This non-linear dependence of the folding rate constants evidenced in chevron plots is generally interpreted as reflecting the accumulation of a folding intermediate [19,22], even if different explanations have been proposed and discussed [23].

We therefore hypothesized that an additional, and even faster folding phase undetectable by SF experiments because of the dead time of the mixing apparatus (2–3 ms), was to be observed under refolding conditions in the sub-ms time regime. Indeed, this hypothesis was experimentally confirmed by T-jump folding experiments carried out under matching temperature conditions (T = 20 °C) at different urea concentrations. The time courses obtained under folding and unfolding conditions were always satisfactorily fitted to a single exponential decay at any denaturant concentration (representative kinetic traces are reported in Fig. S6). The results of these experiments allowed us to measure not only the rate constant relative to the rapid formation of the intermediate, but also the kinetics of its unfolding at higher urea concentration. The data reported in Fig. 3 therefore represent the urea dependence of the main folding phases for BRD2(2) (panel A) and BRD4(1) (panel B): both proteins show a slower process observed by SF experiments and relative to the (un)folding of the native state, and a faster process, observed only by T-jump experiments, describing the rapid folding and unfolding of an intermediate species. However, as thoroughly discussed [19], identification of a transient folding intermediate is not sufficient to assign its kinetic role in a three state mechanism. In particular, an intermediate state may represent an obligatory species toward the formation of the native state ($D \rightleftharpoons I \rightleftharpoons N$; on-pathway intermediate), or a kinetic trap along the folding pathway ($I \rightleftharpoons D \rightleftharpoons N$; off-pathway intermediate). A clear distinction between these two alternative scenarios can be obtained if the urea dependence of all the four rate constants relative to the (un)folding of the native and intermediate species (k_{DI}, k_{ID}, k_{IN} and k_{NI}) are measured over a wide range of urea concentration. Following an approach generally used to analyze the folding mechanism of different proteins [13,19,24,25] we globally fitted the SF and T-jump data reported in the chevron plots to a three-state scheme, involving either an on- and an off-pathway intermediate (Fig. 3A/B). The four microscopic rate constants and the corresponding m-values obtained by this procedure allowed us to assign to the folding intermediate of BRD2(2) and BRD4(1) the role of an on-pathway species along the pathway of folding to the native state, since the off-pathway model fails to adequately fit the data in both cases. It is interesting to notice that an obligatory transient folding intermediate has been described also for the folding mechanism of other, non-related, four helical bundle proteins [13–15,26].

3.3. BRDs folding mechanism

Using the parameters obtained by the fit to the on-pathway model (see legend to Fig. 3), we also determined the populations of the three species at equilibrium as a function of urea concentration. Such an analysis, predicts that the intermediate species identified in the folding mechanism of both BRD domains is only negligible populated at equilibrium (< 1%) at urea concentration corresponding to the midpoint of the folding transition (e.g. [urea] = 5.2 M and 6.4 M for BRD2(2) and BRD4(1), respectively) (data not shown). The kinetic parameters obtained from the on-pathway model were also used to calculate the energy profiles, highlighting the position of the intermediate and transition states along a reaction coordinate. As shown in Fig. 4, both BRDs

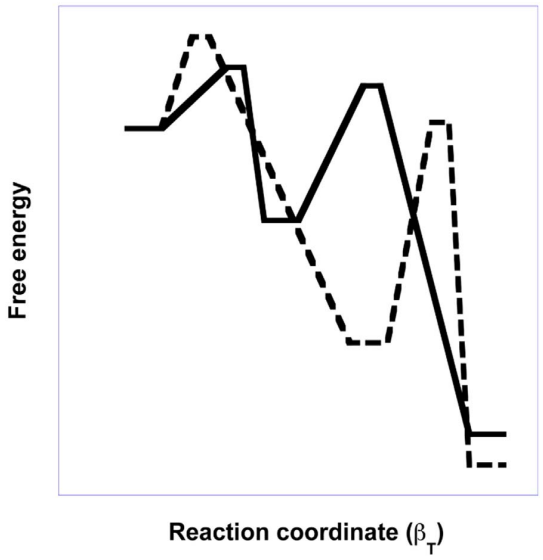

Fig. 4. Schematic energy diagrams for the folding of BRD2(2) (continuous line) and BRD4(1) (dashed line). The free energy values and the β_T values, were calculated from the kinetic parameters obtained by fitting the chevron plots of the two BRD domains to an on pathway intermediate (see the legend to Fig. 3). Free energy values were calculated with the Arrhenius equation using a pre-exponential factor of 4.8×10^8 s^{-1} [15]. BRD2(2): ΔG_{DI} = 1.14 kcal mol^{-1}; ΔG_{DN} = 10.16 kcal mol^{-1}; β_T(TS1) = 0.32; β_T(I) = 0.40; β_T(TS2) = 0.71. BRD4(1): ΔG_{DI} = 6.83 kcal mol^{-1}; ΔG_{DN} = 14.80 kcal mol^{-1}; β_T(TS1) = 0.22; β_T(I) = 0.75; β_T(TS2) = 0.80.

fold along a minimal three-state mechanism involving a denatured-like and a native-like transition states (TS1 and TS2, respectively), and on-pathway intermediate in between. The calculated Tanford β-values (β_T) for TS1, reflecting the buried surface area relative to the unfolded and native states, is β_T = 0.32 for BRD2(2) and β_T = 0.22 for BRD4(1), whereas the β_T for TS2 is 0.71 for BRD2(2) and 0.81 for BRD4(1). These results suggest that the two transition states of the two proteins display similar structural properties. On the contrary, the thermodynamic and conformational properties of the intermediate species appear to be largely different in the two BRDs; in fact, the intermediate populated by BRD4(1) is more stable relative to that of BRD2(2) ($\Delta\Delta G_{DI}$ = 5.7 ± 0.8 kcal mol^{-1}) and is clearly more native-like, as judged by its β_T value relative to the β_T value calculated for BRD2(2) (β_T = 0.7 and β_T = 0.4, respectively). The larger stability of the BRD4(1) intermediate relative to that of the BRD2(2) mirrors the greater stability of its native state ($\Delta\Delta G_{DN}$ = 4.3 ± 1.3 kcal mol^{-1} from kinetic data), suggesting that this intermediate is stabilized by native-like interactions. Moreover, inspection of Fig. 4 shows that the stabilities of the two transition states TS1 and TS2 and the intermediate in between in the folding pathway are correlated, as has been observed analyzing different sets of structurally unrelated proteins following a three-state folding mechanism [19,27]. Altogether, these observations suggest that formation of an intermediate species is a common property of the folding of these two BRDs; nevertheless, specific sequence features appear to be crucial to modulate its stability and conformational properties.

Together with native state topology, inherent propensity to form secondary structural elements is a key factor in modulating the folding process of proteins [28] and its contribution can be clearly evidenced studying the folding mechanism of homologous proteins sharing the same topological properties. In particular, it has been shown that, as the propensity for forming secondary structure increases, the folding mechanism of proteins of the same fold family slides from two-state to multi-state mechanisms [29,30]. In the case of BRD2(2) and BRD4(1), a comparison of helical propensities of sequence elements is meaningful, given the high structural homology between these two proteins. Fig. 5 shows that the distribution of helical propensity (as calculated by

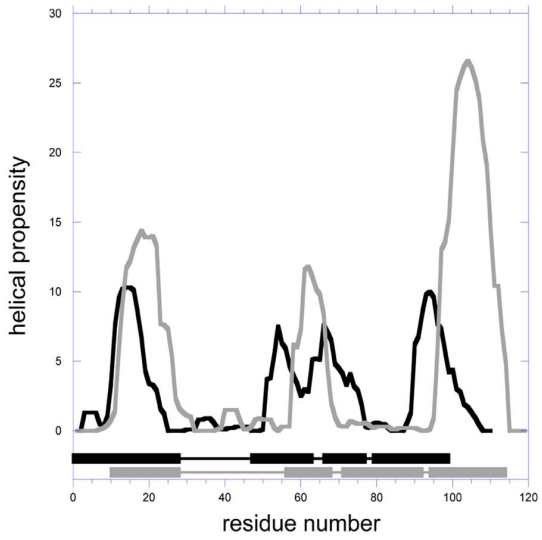

Fig. 5. Helical propensity of BRD2(2) (black line) and BRD4(1) (grey line). Helical propensity was calculated by the AGADIR program [31] (http://agadir.crg.es) Boxes represent the four helices, as determined from the X-ray structure of BRD2(2) (pdb id: 3oni; black boxes) and BRD4(1) (pdb id: 3uvx; grey boxes).

AGADIR [31],) between the two BRDs is very similar but that the overall helical propensity is higher in the case of BRD4(1), particularly at the level of the αC C-terminal helix. Phi-value analysis is in progress and it will allow us to describe the structure of the intermediate and transition states at the residue level and to check whether the C-terminal α−helix is part of the folding nucleus in these two BRDs.

4. Conclusions

A fruitful strategy for extracting general rules governing the folding of proteins is the comparison of the folding mechanism of proteins belonging to the same structural family. In this context, the bromodomains (BRDs) offer an as yet unexplored experimental system to study the folding mechanism of proteins belonging to the all-α fold class. In this paper we have reported the thermodynamic characterization at equilibrium and the folding kinetics of BRD2(2) and BRD4(1), two representative domains of domain 1 and 2 of the BET BRD family. The results reported in this work allow us to propose that formation of an obligatory intermediate may be a general feature of the folding landscape explored by these small all-α domains and add general significance to the hypothesis that members of a given fold family share a consensus folding mechanism. Our observations, however, highlight that the intermediate species populated during the folding of BRD4(1) is closer to the native state along the reaction coordinate than that populated by the less stable BRD2(2). This conclusion, which will be corroborated by structural analysis of folding intermediate(s) and transition states, underscores the role played by the sequence in modulating the stability of transiently populated states.

Acknowledgements

We thank Prof. Stefan Knapp (Institute for Pharmaceutical Chemistry and Buchmann Institute for Life Sciences (BMLS), Johann Wolfgang Goethe-University, Frankfurt am Main, Germany) for kindly providing us with the plasmids harboring the BRDs wild type genes. Work partially supported by grant C26A14AXLE – Sapienza Università di Roma to C.T.A. and by grant Regione Lazio (Prot. FILAS-RU-2014-1020) to V.C.

Appendix A. Transparency document

Transparency document associated with this article can be found in the online version at http://dx.doi.org/10.1016/j.bbrep.2017.06.009.

Appendix B. Supporting information

Supplementary data associated with this article can be found in the online version at http://dx.doi.org/10.1016/j.bbrep.2017.06.009.

References

[1] T. Kouzarides, Cell 128 (2007) 693–705.
[2] R. Chandrasekaran, M. Thompson, Biochem. Biophys. Res. Commun. 355 (2007) 661–666.
[3] F. Gong, L.Y. Chiu, K.M. Miller, PLoS Genet. 12 (2016) e1006272.
[4] M.Y. Lubula, B.E. Eckenroth, S. Carlson, A. Poplawski, M. Chruszcz, K.C. Glass, FEBS Lett. 588 (2014) 3844–3854.
[5] P. Filippakopoulos, J. Qi, S. Picaud, Y. Shen, W.B. Smith, O. Fedorov, E.M. Morse, T. Keates, T.T. Hickman, I. Felletar, M. Philpott, S. Munro, M.R. McKeown, Y. Wang, A.L. Christie, N. West, M.J. Cameron, B. Schwartz, T.D. Heightman, N. La Thangue, C.A. French, O. Wiest, A.L. Kung, S. Knapp, J.E. Bradner, Nature 468 (2010) 1067–1073.
[6] P. Filippakopoulos, S. Picaud, M. Mangos, T. Keates, J.P. Lambert, D. Barsyte-Lovejoy, I. Felletar, R. Volkmer, S. Muller, T. Pawson, A.C. Gingras, C.H. Arrowsmith, S. Knapp, Cell 149 (2012) 214–231.
[7] L.L. Fu, M. Tian, X. Li, J.J. Li, J. Huang, L. Ouyang, Y. Zhang, B. Liu, Oncotarget 6 (2015) 5501–5516.
[8] C.N. Chi, S.R. Haq, S. Rinaldo, J. Dogan, F. Cutruzzola, A. Engstrom, S. Gianni, P. Lundstrom, P. Jemth, Biochemistry 51 (2012) 8971–8979.
[9] S. Gianni, J. Dogan, P. Jemth, Biophys. Chem. 189 (2014) 33–39.
[10] S.L. Shammas, M.D. Crabtree, L. Dahal, B.I. Wicky, J. Clarke, J. Biol. Chem. 291 (2016) 6689–6695.
[11] C. Kupitz, R. Chandrasekaran, M. Thompson, Biophys. Chem. 136 (2008) 7–12.
[12] S. Picaud, M. Strocchia, S. Terracciano, G. Lauro, J. Mendez, D.L. Daniels, R. Riccio, G. Bifulco, I. Bruno, P. Filippakopoulos, J. Med. Chem. 58 (2015) 2718–2736.
[13] A. Borgia, D. Bonivento, C. Travaglini-Allocatelli, A. Di Matteo, M. Brunori, J. Biol. Chem. 281 (2006) 9331–9336.
[14] A.P. Capaldi, M.C.R. Shastry, C. Kleanthous, H. Roder, S.E. Radford, Nat. Struct. Biol. 8 (2001) 68–72.
[15] K. Teilum, K. Maki, B.B. Kragelund, F.M. Poulsen, H. Roder, Proc. Natl. Acad. Sci. USA 99 (2002) 9807–9812.
[16] Z. Zhou, Y. Huang, Y. Bai, J. Mol. Biol. 352 (2005) 757–764.
[17] L. Lori, A. Pasquo, C. Lori, M. Petrosino, R. Chiaraluce, C. Tallant, S. Knapp, V. Consalvi, PLos One 11 (2016).
[18] M.M. Santoro, D.W. Bolen, Biochemistry 27 (1988) 8063–8068.
[19] S. Gianni, Y. Ivarsson, P. Jemth, M. Brunori, C. Travaglini-Allocatelli, Biophys. Chem. 128 (2007) 105–113.
[20] M.J. Parker, J. Spencer, A.R. Clarke, J. Mol. Biol. 253 (1995) 771–786.
[21] T. Kiefhaber, F.X. Schmid, J. Mol. Biol. 224 (1992) 231–240.
[22] I.E. Sanchez, T. Kiefhaber, J. Mol. Biol. 325 (2003) 367–376.
[23] M. Oliveberg, Acc. Chem. Res. 31 (1998) 765–772.
[24] C. Travaglini-Allocatelli, S. Gianni, M. Brunori, Trends Biochem. Sci. 29 (2004) 535–541.
[25] C. Travaglini-Allocatelli, S. Gianni, V.K. Dubey, A. Borgia, A. Di Matteo, D. Bonivento, F. Cutruzzola, K.L. Bren, M. Brunori, J. Biol. Chem. 280 (2005) 25729–25734.
[26] D.M. Korzhnev, T.L. Religa, W. Banachewicz, A.R. Fersht, L.E. Kay, Science 329 (2010) 1312–1316.
[27] K. Kamagata, K. Kuwajima, J. Mol. Biol. 357 (2006) 1647–1654.
[28] A.A. Nickson, J. Clarke, Methods 52 (2010) 38–50.
[29] V. Daggett, A.R. Fersht, Trends Biochem. Sci. 28 (2003) 18–25.
[30] S. Gianni, N.R. Guydosh, F. Khan, T.D. Caldas, U. Mayor, G.W.N. White, M.L. DeMarco, V. Daggett, A.R. Fersht, Proc. Natl. Acad. Sci. USA 100 (2003) 13286–13291.
[31] V. Munoz, L. Serrano, Nat. Struct. Biol. 1 (1994) 399–409.